Desalination and Water Treatment
www.deswater.com
doi: 10.1080/19443994.2015.1070764

57 (2016) 15133–15145
July

Taylor & Francis
Taylor & Francis Group

Iron oxide-impregnated dextrin nanocomposite: synthesis and its application for the biosorption of Cr(VI) ions from aqueous solution

Alok Mittal[a,*], Rais Ahmad[b], Imran Hasan[b]

[a]*Department of Chemistry, Maulana Azad National Institute of Technology, Bhopal 462003, India, Tel. +91 9425025427; Fax: +91 755 2670562; email: aljymittal@yahoo.co.in*
[b]*Environmental Research Laboratory, Department of Applied Chemistry, Aligarh Muslim University, Aligarh 202002, India*

Received 26 May 2015; Accepted 1 July 2015

ABSTRACT

In this paper, iron oxide impregnated with dextrin (Dex-Fe_3O_4) nanocomposite was synthesized by simple one-step hydrothermal chemical precipitation reaction. The nanocomposite was characterized by XRD, FT-IR, TGA, DTG, SEM with EDX and TEM techniques. The material was further explored as an adsorbent for the removal of Cr(VI) ions from its aqueous solution. The optimum removal of Cr(VI) ions with the highest adsorption capacity of 17.8 mg g^{-1} was observed at pH 2. The equilibrium data were analysed with Langmuir, Freundlich, D–R and Temkin isotherms model and data were best followed by Langmuir model and Temkin model with a maximum monolayer adsorption capacity of 51.28, 54.64, and 71.43 mg g^{-1} at 30, 40, and 50°C, respectively. The activation energy calculated by D–R model reveals that the adsorption process is chemisorption in nature. The experimental data were best fitted with pseudo-second-order. The results of thermodynamic parameters (ΔG°, ΔH°, and ΔS°) showed that the adsorption of Cr(VI) on Dex-Fe_3O_4 is endothermic spontaneous in nature. The synthesized nanocomposite material is very promising for the removal of Cr(VI) from aqueous solution.

Keywords: Dex-Fe_3O_4; TEM; FT-IR; Activation energy; Endothermic

1. Introduction

Among various heavy metals, Cr(VI) is one of the most important heavy metal due to its vast applications in industries [1,2]. In aqueous medium, two forms of chromium exists, i.e. Cr(III) and Cr(VI) and the toxicity and reactivity of both the forms mainly depend on oxidation state of the chromium [3]. In trace amounts, Cr(III) is an essential nutrient for humans and to mammals for their maintenance of normal glucose tolerance factor, lipid and protein metabolism [4]. On the other hand, Cr(VI) is very toxic to human as well as marine life and poses various health problems such as liver damage and pulmonary congestion and regarded as carcinogenic also [5–7].

Various conventional methods have been developed for the removal of Cr(VI) in wastewater, including electrochemical precipitation, ion exchange, membrane ultrafiltration, reverse osmosis, reduction and adsorption [8–10]. Of these methods, adsorption has been widely used for the removal of chromium from contaminated groundwater [11] due to its low initial cost and ease of operation and high efficiency to remove such toxic heavy metals. This technique can

*Corresponding author.

be utilized for large scale of polluted water frequently as it can handle fairly large flow rates, producing a high quality of water without producing notorious sludge and residual contaminants [12–14].

Recently, Fe_3O_4 nanoparticles have been used as a highly efficient material for the removal of heavy metals by adsorption due to its excellent magnetic properties, chemical stability, and biocompatibility and large surface area [15–17]. However, difficulty arises due to its nanosize of magnetic particles that agglomerate in contact of aqueous system. To overcome this difficulty, the magnetic nanoparticles were functionalized by polymers and biopolymer having long chain that provides chemical stability and well distribution of MNPs in aqueous system [18,19].

In this study, MNPs were functionalized by a carbohydrate polymer, dextrin which is a mixtures of linear *a*-(1,4)-linked D-glucose polymers [20,21]. Dextrin is a class of low molecular weight carbohydrates produced by acid or/and enzymatic partial hydrolysis of starch or glycogen and is widely used material with a great variety of applications such as adhesives, foods, textiles and cosmetics [22]. So the encapsulation of nanoparticles with dextrin increases the particles dispersion, biocompatible and chemical stability and adsorption efficiency by providing –OH groups on dextrin which can be responsible for an increase in adsorption capacity.

In present study, iron oxide-impregnated dextrin (Dex-Fe_3O_4) nanocomposite were synthesized by simple and inexpensive one-step hydrothermal chemical precipitation reaction and used as an effective adsorbent for the treatment of Cr(VI) ions from the aqueous solution. The prepared Dex-Fe_3O_4 was characterized by Fourier transform infrared (FT-IR) spectroscopy, X-ray diffractometry, scanning electron microscopy, transmission electron microscopy and thermal studies. The effect of pH, Dex-Fe_3O_4 doses, initial concentration of Cr(VI) ions, the kinetics of adsorption and the adsorption isotherms were studied.

2. Experimental

2.1. Chemicals and reagents

Dextrin (Sigma-Aldrich, India), $FeCl_3{\cdot}6H_2O$ and $FeCl_2{\cdot}4H_2O$ (Merck, India), potassium dichromate (Sigma-Aldrich, India), and liquor ammonia (Fischer Scientific, India) were used as received without further purification. Buffer tablets of pH 4.0 and 9.2 were used as received. The stock solution (1,000 mg L^{-1}) of Cr(VI) was prepared by dissolving appropriate amount of $K_2Cr_2O_7$ in double-distilled water.

2.2. Synthesis of Dex-Fe_3O_4 nanocomposite

Dex-Fe_3O_4 nanocomposite was synthesized by a simple one-step chemical co-precipitation method followed by treatment under hydrothermal conditions [23]. Briefly, 4.8 gm of $FeCl_2{\cdot}4H_2O$, 9.5 gm of $FeCl_3{\cdot}6H_2O$ and 5.5 g of dextrin were dissolved in 150 mL of double-distilled water with vigorous stirring at a speed of 1,000 rpm for 2 h. 20 mL of 25% solution liquor ammonia (NH_4OH) was added after the solution was heated to 90˚C. The reaction was continued for 2 h at 90˚C under constant stirring and nitrogen environment. The resulting nanoparticles were then centrifuged and washed with double-distilled water four to five times to remove any unreacted chemicals and dried in a vacuum oven at 60˚C for 2 h.

2.3. Characterization of Dex-Fe_3O_4 nanocomposite

The modification of Fe_3O_4 MNPs with dextrin was confirmed by different techniques such as FT-IR, X-ray diffraction (XRD), scanning electron microscopy and transmission electron microscopy.

The nanocomposite was characterized by FT-IR and spectra were recorded in transmission mode (Perkin Elmer 1800 model) on powder samples that were ground with KBr and compressed into a pellet. FT-IR spectra in the range 4,000–400 cm^{-1} were recorded in order to investigate the structural determination and bond formation.

XRD patterns of the samples were obtained using Siemens D 5005 X-ray unit Cu Kα (λ = 1:5,406 Å) radiation, generated at a voltage of 40 kV and a current of 40 mA.

The changes in the morphology of dextrin after the incorporation of Fe_3O_4 MNPs were studied using scanning electron microscope (GSM 6510LV) under a 20-kV electron acceleration voltage coupled with energy dispersive (EDX) for elemental analysis. The particle size and structure of the synthesized nanocomposite were observed using JEM 2100 transmission electron microscope (TEM).

The thermal stability was determined by thermogravimetric analysis (TGA, Perkin Elmer model, STA 6000) and derivative thermal analysis (DTG, Perkin Elmer Pyris 6). The TGA thermograms were recorded for 20 mg of powder sample at a heating rate of 10˚C min^{-1} in the temperature range of 30–800˚C under nitrogen atmosphere.

Atomic absorption spectrophotometer (AAS) model GBC-902 was used to investigate the concentration of metal ions in the supernatant. Elico Li 120 pH meter was used to adjust the pH of the solutions.

2.4. Adsorption experiments

The adsorption experiments were carried out using batch equilibrium technique in aqueous solutions at a pH range of 2–3 and at temperature range 30–50°C. 50 mg of magnetic nanoadsorbents was added to 20 mL of Cr(VI) solution of various concentrations (from 10 to 100 mg L^{-1}) and shaken in a thermostatic water-bath shaker operated at 120 rpm. After equilibrium was reached, magnetic nanoadsorbents were removed and the supernatant was collected after reaching equilibrium. The concentrations of Cr(VI) in supernatant were measured using flame AAS. The solution pH was adjusted by 0.1 M NaOH or HCl. Kinetic experiments were performed at three different Cr(VI) ion concentrations mainly at 10, 50, and 100 mg L^{-1} at pH range of 2–3. The effect of time on the adsorption of Cr(VI) ions on Dex-Fe_3O_4 nanocomposite was studied at 5–360 min and equilibrium time was reached at 180 min. The effect of adsorbent dose and initial metal ion concentration was also studied. The amount of metal ions adsorbed onto Dex-Fe_3O_4 was calculated by well-known mass balance relationship.

3. Results and discussion

3.1. Characterization of Dex-Fe_3O_4 nanocomposite

The functionalization of dextrin on magnetic nanoparticles was confirmed by FTIR spectroscopy. Fig. 1 shows the FTIR spectra of Fe_3O_4 MNPs, dextrin and dextrin-functionalized Fe_3O_4 nanocomposite in the range 4,000–400 cm^{-1} wavenumber range. Spectrum of Fe_3O_4 MNPs shows a high-intensity band at 578 cm^{-1} corresponds to the Fe–O stretching vibration from the magnetite [24], and bands at 1,631, 3,393 cm^{-1} can be assigned to the O–H stretching modes and bending vibration of Fe_3O_4, respectively. FTIR of dextrin showed a broad peak at 3,437 cm^{-1}which is due to O–H stretching. This broad band indicates association due to –OH groups (Fig. 1). Other important peaks were observed at 2,934 cm^{-1} (aliphatic C–H stretching), 1,733 cm^{-1} (C–O stretching) and 1,000–1,158 cm^{-1} (C–O–C stretching) [25]. The spectra of the iron oxide nanoparticles functionalized with dextrin exhibit few differences as compared to pure dextrin and Fe_3O_4 MNPs, which indicates that the interactions between dextrin and iron oxide MNPs are intermolecular interactions.

Fig. 2 shows the XRD patterns of Fe_3O_4 MNPs, dextrin and Dex-Fe_3O_4 nanocomposite. Core Fe_3O_4 MNPs diffraction peaks were observed at 30.4370, 31.8948, 35.8414, 43.4590, 53.8936, 57.3527, 62.9424, and 74.4688 at 2θ scale and for dextrin 22.9658, 30.4666, 38.3965, and 72.6042. The Dex-Fe_3O_4 nanocomposite shows diffraction peaks at 30.1882, 33.2602, 35.5757, 43.2436, and 57.4402 that are characteristic peaks of Fe_3O_4 MNPs with little bit shift of the peaks towards lower 2θ value showing that the MNPs are modified with dextrin. The crystalline structure of core Fe_3O_4 MNPs changes slightly in Dex-Fe_3O_4 nanocomposite due to modification with dextrin.

Thermal stability of dextrin and Dex-Fe_3O_4 was checked by thermogravimetric analysis and derivative weight loss and the curves are shown in Figs. 3 and 4. It can be seen from the Fig. 3 that dextrin shows a weight loss of 10% at 108.63°C due to loss of free water. In the temperature range of 237–327°C, the main degradation of dextrin was seen with 60–70% of weight loss. This weight loss may be due to selective dehydration, possibly accompanied by transglucosidation. A residual

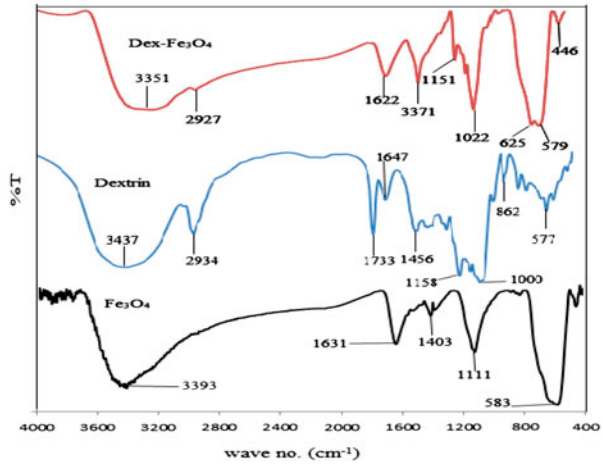

Fig. 1. FT-IR spectra of Fe_3O_4 MNPS, dextrin and Dex-Fe_3O_4 nanocomposites.

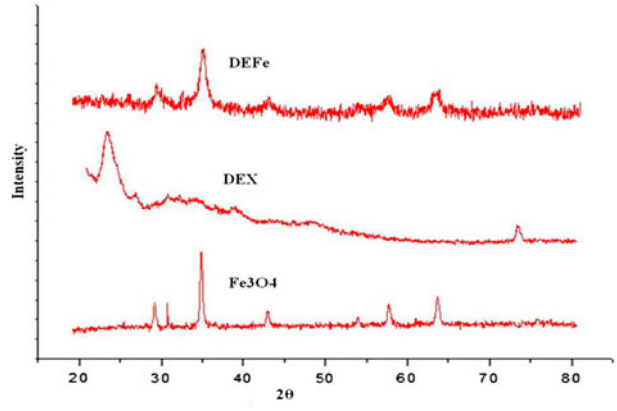

Fig. 2. XRD patterns of Fe_3O_4 MNPS, dextrin and Dex-Fe_3O_4 nanocomposites.

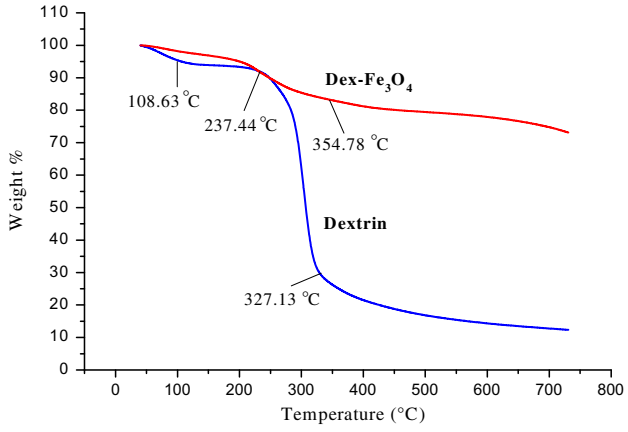

Fig. 3. Thermograms for dextrin and Dex-Fe_3O_4 nanocomposites.

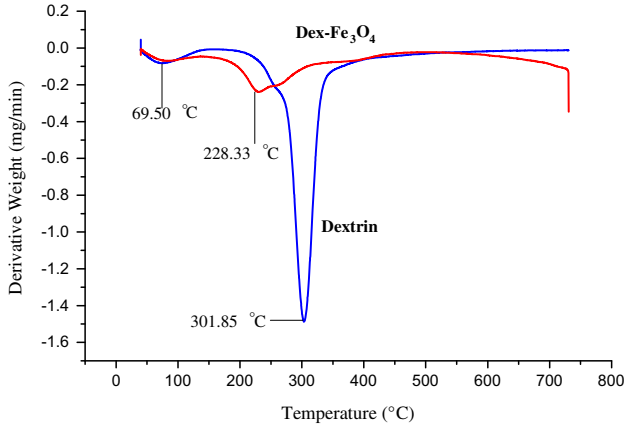

Fig. 4. DTG thermogram of dextrin and Dex-Fe_3O_4.

mass of 15% was obtained at 500°C for dextrin. While looking at the thermogram of Dex-Fe_3O_4 nanocomposite, it is found that the weight loss curve of the nanocomposite is continuous and occurs at a higher temperature than pure dextrin confirming that the Fe_3O_4 MNPs have been reinforced in the biopolymer matrix. Also, the weight loss of the nanocomposite material is very less (25%) as compared to pure dextrin (80%). So reinforcement of Fe_3O_4 MNPs in the dextrin matrix provides a good thermal stability to the biopolymer. Thermal stability of the dextrin and its nanocomposite can also be analysed by derivative thermogram as shown in inset of Fig. 4. In the thermogram, the melting temperature of dextrin was found at 301°C which is due to elimination of polyhydroxyl groups, in association with de-polymerization and decomposition [26], while for Dex-Fe_3O_4 nanocomposite, the melting temperature (T_m) was observed at 228.33°C. This shift in T_m could be attributed to rearrangement in the distribution of molecular weight and transformation of the crystallinity of dextrin due to reinforcement of Fe_3O_4 MNPs in dextrin matrix.

Scanning electron micrographs of dextrin, Dex-Fe_3O_4 (before adsorption) with its EDS and Dex-Fe_3O_4 loaded with Cr(VI) with its EDS are shown in Fig. 5. The dextrin granules were spherical with a smooth surface and after reinforcement with Fe_3O_4 MNPs, it shows porous structure showing a narrow size distribution of nanoparticles within the matrix of biopolymer. The change in morphology is due to formation of a crosslink network between dextrin and Fe_3O_4 MNPs. After adsorption, the morphology of Dex-Fe_3O_4 nanocomposite again changes due to swelling of water as shown in Fig. 6.

Typical TEM image of Dex-Fe_3O_4 nanocomposite has been shown in Fig. 7 which indicates the presence of relatively spherical structures and well-dispersed distribution of the Fe_3O_4 MNPs in the dextrin matrix. According to the Fig. 6, the average size of Fe_3O_4 MNPs was estimated to be 4.96 nm.

3.2. Sorption behaviour of Cr(VI) onto Dex-Fe_3O_4

3.2.1. Effect of contact time and initial metal ion concentration

The effect of retention time on removal efficiency of Cr(VI) was investigated by varying the contact time in the range of 5–300 min at three different metal ion concentrations 10, 50, and 100 mg L^{-1} at pH 2 and adsorbent dose of 50 mg. The effect of contact time on Dex-Fe_3O_4 for Cr(VI) removal is depicted in Fig. 8 indicating an initial increase in adsorption capacity with an increase in time and attaining the equilibrium time at 180 min after that little change in adsorption capacity for Cr(VI) is seen which indicates that the system has already achieved equilibrium. No change in adsorption capacity after equilibrium reveals that the adsorption sites are completely occupied by metal ion.

The initial metal ion concentration provides an important driving force to overcome all mass transfer resistance of metal ions between the aqueous and solid phases [27]. Three different concentrations 10, 50, and 100 mg L^{-1} of the metal ions were chosen to see the effect of initial metal ion concentration on adsorption capacity of Dex-Fe_3O_4. Fig. 8 also shows the effect of initial metal ion concentration in which by increasing Cr(VI) ions concentration, the adsorption capacity continuously increases. The maximum adsorption capacity at 10, 50, and 100 mg L^{-1} was found to be 9.88, 18.56, and 31.77 mg g^{-1}, respectively which might be due to the fact that increasing metal

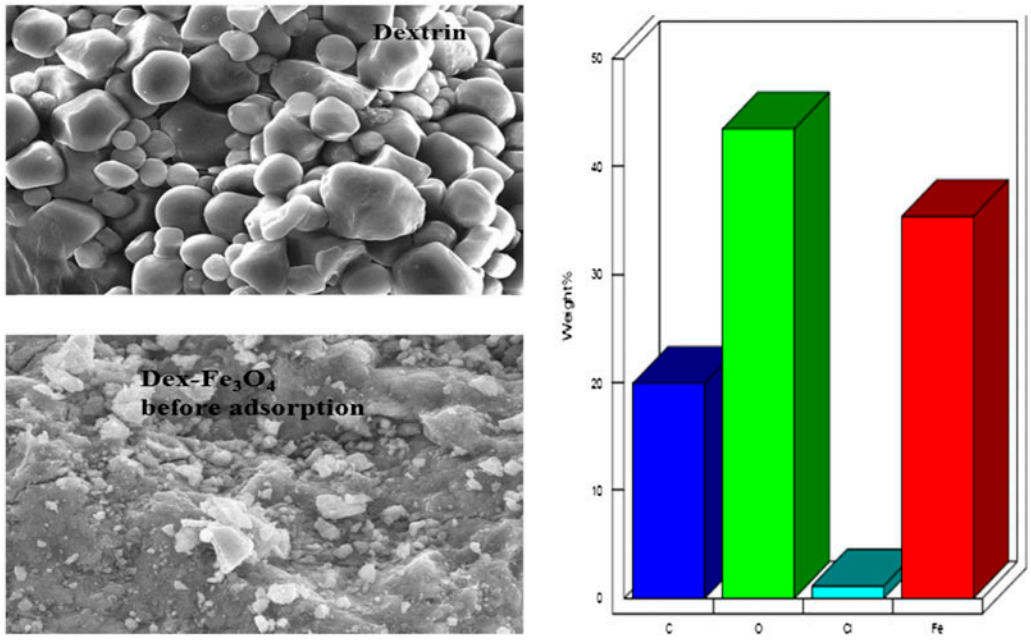

Fig. 5. SEM images of dextrin and Dex-Fe_3O_4 nanocomposites with its EDS before adsorption.

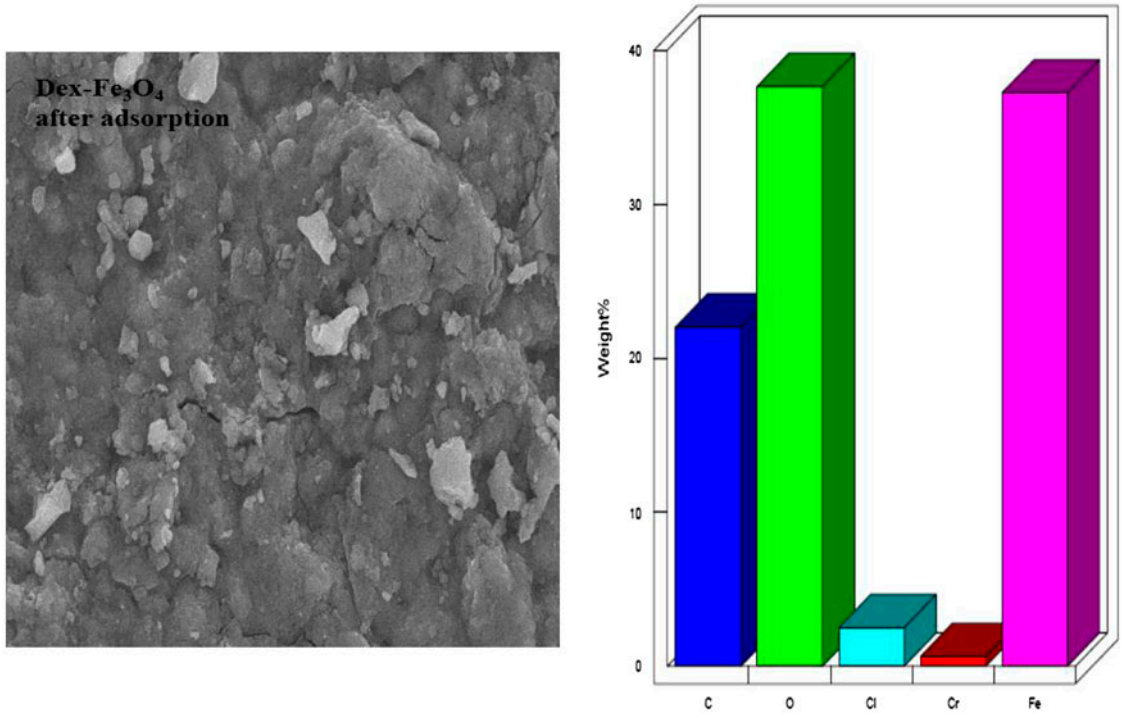

Fig. 6. SEM image of Dex-Fe_3O_4 nanocomposite with its EDS after adsorption.

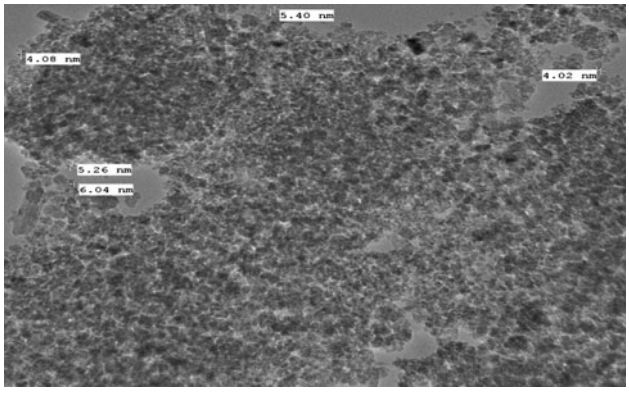

Fig. 7. TEM image of Dex-Fe_3O_4 nanocomposite showing particle size and particle distribution.

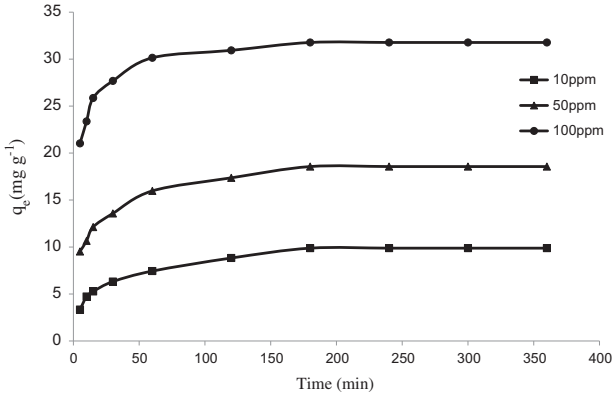

Fig. 8. Effect of contact time for the removal of Cr(VI).

ion concentration increased the number of collision between the adsorbent and metal ion species, this leading an increased metal uploading [28].

3.2.2. Effect of pH

One the most important parameter that directly affects the adsorption of Cr(VI) is pH. The effect of the initial solution pH on the removal of Cr(VI) was studied with 50 mg of Dex-Fe_3O_4 nanocomposite, 20 mL of 50 mg L^{-1} Cr(VI) solution with different pH values in the range 2–7at 30˚C. The effect of pH on sorption of Cr(VI) has been shown in Fig. 9. It was found that the maximum adsorption capacity for Cr (VI) was in the pH value of 2 and as the pH value increases, the adsorption capacity decreases. Various forms of Cr(VI) in water such as $HCrO_4^-$ in acidic medium, CrO_4^{2-} in neutral and basic medium are predominant factors for the adsorption of Cr(VI) onto Dex-Fe_3O_4 nanocomposite.

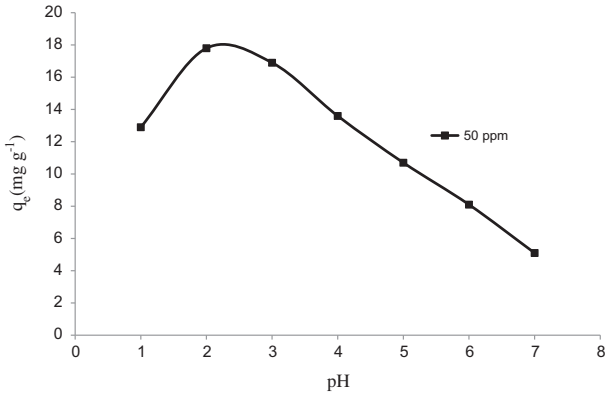

Fig. 9. Effect of pH for the removal of Cr(VI).

At pH < 4, due to the presence of excess of H^+ ions in the solution, the adsorbent surface becomes positively charged due to protonation and $HCrO_4^-$ form of Cr(VI) ions are dominant at lower pH [29], so strong electrostatic attraction between positively charged adsorbent surface and negatively charged $HCrO_4^-$ ions leads to higher removal efficiency. However, as the pH increases, deprotonation of surface of the adsorbent was occurred due to the decrease in the number of H^+ ions. So lower adsorption capacity results due to less interaction between Cr(VI) ions and adsorbent surface at higher pH value. The point of zero charge of adsorbent surface is found to be 5.5.

3.2.3. Effect of adsorbent dose and temperature

To investigate the effect of adsorbent amount for Cr(VI) removal, various amounts of adsorbent dose from 10 to 100 mg was used at 30˚C with 20 mL of 50 mg L^{-1} Cr(VI) solution at pH 2. The sample was agitated in a shaker at 120 rpm and after 180 min the adsorption capacity was calculated. From Fig. 10, it can be seen that the adsorption capacity increases with an increase in the adsorbent amount till 70 mg after that slight increase in adsorption capacity was observed. This trend can be explained as the adsorbent dose increases, the number of adsorbent particles also increases facilitating more active sites for adsorption. However, as the amount of adsorbent increases, effective surface area and adsorbate/adsorbent ratio reduce resulting in less metal ion uptake. In our study, 50-mg adsorbent dose was used for further experiments.

Due to the influence of temperature on adsorption of Cr(VI) ions, experiments were performed at 30, 40, and 50˚C with 20 mL of 50 mg L^{-1} Cr(VI) solution in a water-bath shaker incubator (120 rpm) for 180 min.

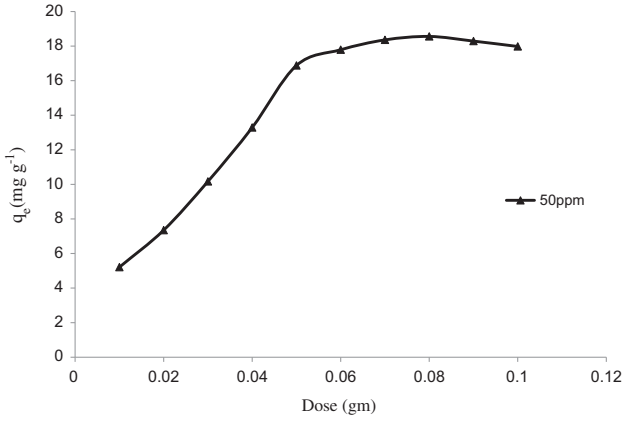

Fig. 10. Effect of adsorbent dosage for the removal of Cr(VI).

It was seen that by increasing the temperature, the adsorption capacity of the adsorbent also increases showing that the adsorption of Cr(VI) onto Dex-Fe_3O_4 nanocomposite follows an endothermic process and could be elucidated by activation of the adsorbent surface at higher temperatures. This could also be due to the easily mobility of heavy metals ions from the bulk solution towards the adsorbent surface and enhanced the accessibility to the adsorbent active sites at higher temperature [30].

3.3. Adsorption isotherms

To investigate the interaction between metal ion and adsorbent, three well-known adsorption isotherms viz. Langmuir [31], Freundlich [32] and Dubinin–Radushkevich (D–R) [33] and Temkin were used to fit the experimental data and describe the isotherm constants of metal ion uptake by adsorbents.

The Langmuir equation is generally used to calculate the maximum adsorption capacity corresponding to the complete monolayer coverage on homogenous adsorbent surface without any interaction between the adsorbed ions. Linearized Langmuir equation is commonly represented as;

$$\frac{c_e}{q_e} = \frac{1}{q_m K_L} + \frac{c_e}{q_m} \tag{1}$$

where c_e is the equilibrium concentration of metal ions (mg L^{-1}), q_e is the adsorption amount at the equilibrium (mg g^{-1}), q_m is the maximum capacity (mg g^{-1}) and K_L is the Langmuir constant related to the affinity of binding sites (L mg^{-1}).

The linearized Freundlich equation can be represented as;

$$\ln q_e = \frac{1}{n} \ln c_e + \ln K_F \tag{2}$$

where K_F is roughly an indicator of the adsorption capacity and n is the adsorption intensity which is a numerical value and varies with heterogeneity. The magnitude of the exponent n gives an indication of the favourability of adsorption. For a favourable adsorption, the value of n must be greater than unity.

D–R isotherm is generally applied to express the adsorption mechanism with a Gaussian energy distribution onto a heterogeneous surface. The isotherm is generally expressed by the following equation:

$$\ln q_e = \ln q_m - \beta \varepsilon^2 \tag{3}$$

where q_e is the amount of metal ion adsorbed on the adsorbent at equilibrium (mg g^{-1}); q_m is the theoretical isotherm saturation capacity (mg g^{-1}); β is the D–R isotherm constant (mol^2 kJ^{-2}) and ε is the D–R isotherm constant. The model is generally used to distinguish the physical and chemical adsorption of metal ions with its mean free energy, E per molecule of adsorbate can be computed by the relationship;

$$E = \frac{1}{\sqrt{2\beta}} \tag{4}$$

ε is Polanyi potential which is related to the equilibrium concentration as follows:

$$\varepsilon = RT\left(1 + \frac{1}{c_e}\right) \tag{5}$$

where R, T, and c_e represent the gas constant (8.314 J mol^{-1} K^{-1}), absolute temperature (K) and metal ion equilibrium concentration (mg L^{-1}) at equilibrium, respectively.

The Temkin model isotherm contains a factor that explicitly taking into account of adsorbent–adsorbate interactions. The linear equation for the model is given as

$$q_e = B \ln A + B \ln c_e \tag{6}$$

where A is the binding constant corresponding to binding energy in L mg^{-1} and B is the heat of adsorption in J mol^{-1}.

The linear plots for all the four models are given, respectively, in Figs. 11–14 and data calculated from plots are given in Table 1. For all the models, data

were calculated at three different temperatures viz. 30, 40, and 50°C. As can be seen from the Table 1, Langmuir with a higher correlation coefficient (R^2) value 0.99 is assumed to be followed by adsorption process than the other models giving a maximum adsorption capacity of 51.43 at 30°C, 54.64 at 40°C and 71.43 at 50°C. The value of n obtained by Freundlich model at all temperature ranges 30–50°C gives a value greater than unity indicating the adsorption to be favourable. Higher value of n tends to stronger value of interaction between metal ion and adsorbent. As can be seen from Table 1 as the temperature increases, the value of n also increases indicating adsorption is more favourable at high temperature. The value of mean free energy E calculated by D–R isotherm indicates that the adsorption follows a physisorption to chemisorption process as the temperature increases from 30 to 50°C. The increase in binding constant A of Temkin model with respect to temperature indicates an increase in adsorbent–adsorbate interaction at higher temperature. The values of B obtained are continuously decreasing with an increase in temperature indicating an increase in surface coverage at higher temperature. The regression coefficient values obtained also confirm that the model fits to experimental data along with Langmuir model.

3.4. Adsorption kinetics

Adsorption reactions are always time dependent and therefore predicting the rate of the reaction is the most important factor to describe the kinetics of adsorption. Pseudo-first-order, pseudo-second-order [34] and intraparticle diffusion models were used to test the kinetics of adsorption and the rate of the reaction for Cr(VI) on Dex-Fe_3O_4 nanocomposite.

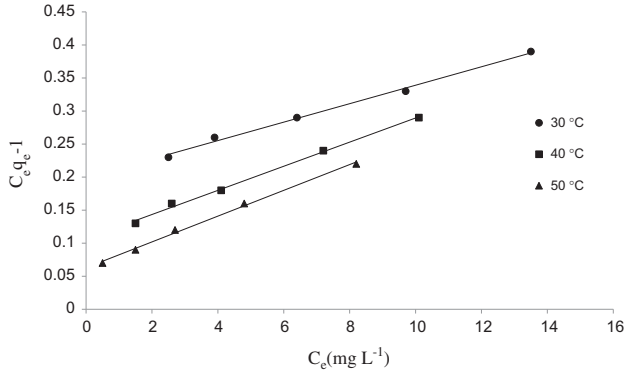

Fig. 11. Langmuir adsorption isotherm for Cr(VI) on Dex-Fe_3O_4 at 30, 40, and 50°C and 50 mg L^{-1} as initial metal ion concentration with 50-mg adsorbent dosage at pH 2.

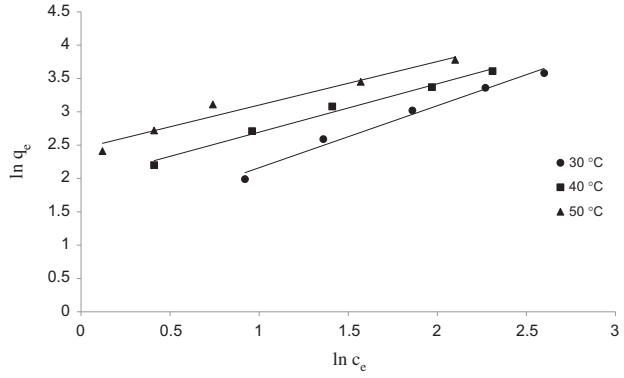

Fig. 12. Freundlich adsorption isotherm for Cr(VI) on Dex-Fe_3O_4 at 30, 40, and 50°C and 50 mg L^{-1} as initial metal ion concentration with 50-mg adsorbent dosage at pH 2.

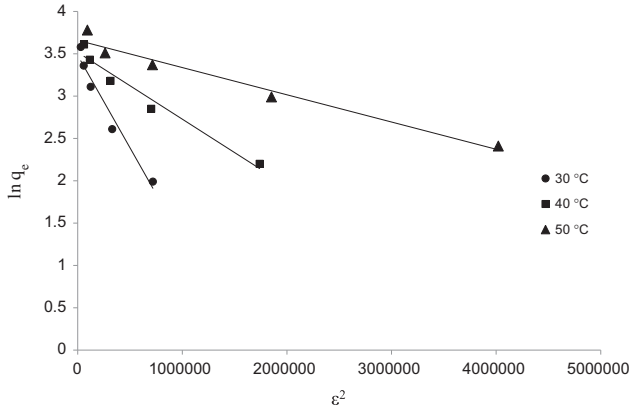

Fig. 13. D–R adsorption isotherm for Cr(VI) on Dex-Fe_3O_4 at 30, 40, and 50°C and 50 mg L^{-1} as initial metal ion concentration with 50-mg adsorbent dosage at pH 2.

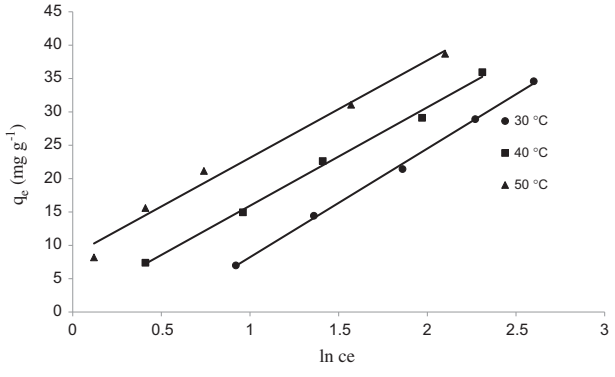

Fig. 14. Temkin isotherm for removal of Cr(VI) on Dex-Fe_3O_4 nanocomposite at 30, 40, and 50°C and 50 mg L^{-1} as initial metal ion concentration with 50-mg adsorbent dosage at pH 2.

Table 1
Adsorption parameters for Cr(VI) ion onto Dex-Fe_3O_4 nanocomposite at 30, 40 and 50°C

Ion	Temperature (°C)	Langmuir			Freundlich			D–R			Temkin		
		q_m	K_L	R^2	n	K_F	R^2	q_m	β	E	R^2	A	B	R^2
Cr(VI)	30	51.43	0.07	0.99	1.08	3.43	0.98	32.43	2×10^6	8.26	0.96	1.08	16.28	0.99
	40	54.64	0.17	0.99	1.38	7.17	0.98	33.68	8×10^7	10.05	0.96	1.64	14.75	0.99
	50	71.43	0.31	0.99	1.53	11.59	0.96	38.81	3×10^7	13.51	0.96	1.79	14.56	0.98

Note: q_m (mg g^{-1}), K_L (L mg^{-1}), K_F [mg g^{-1}(L/mg)$^{1/n}$], β (mol^2 kJ^{-2}), E (kJ mol^{-1}), A (L mg^{-1}), B (J mol^{-1}).

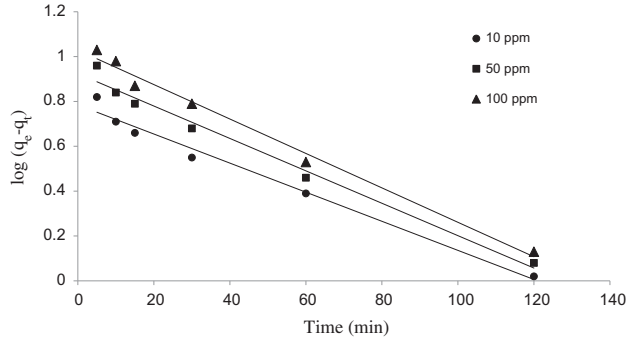

Fig. 15. Pseudo-first-order plot for removal of Cr(VI) onto Dex-Fe_3O_4 nanocomposite at various metal ion concentrations with 50-mg adsorbent dosage and pH 2 at 30°C.

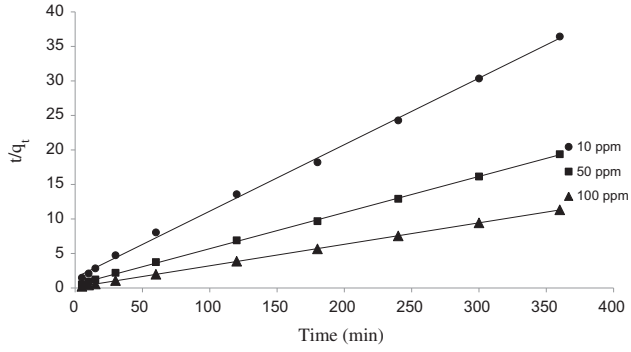

Fig. 16. Pseudo-second-order plot for removal of Cr(VI) onto Dex-Fe_3O_4 nanocomposite at various metal ion concentrations with 50-mg adsorbent dosage and pH 2 at 30°C.

The linear equation for pseudo-first-order model is given as:

$$\log(q_e - q_t) = \log q_e - \frac{k_1}{2.303} t \tag{7}$$

where q_e (mg g^{-1}) is the equilibrium adsorption capacity, q_t (mg g^{-1}) is the adsorption capacity at time t and k_1 (min^{-1}) is the pseudo-first-order rate constant. Values of k_1 and q_e can be obtained from the slope and intercept of the plot of $\log(q_e - q_t)$ and t is given in Fig. 15.

Pseudo-second-order rate equation is given as:

$$\frac{t}{q_t} = \frac{1}{k_2 q_e^2} + \frac{t}{q_e} \tag{8}$$

where k_2 is the pseudo-second-order rate constant (g mg^{-1} min^{-1}), q_e is the amount of Cr(VI) ions

Table 2
Kinetic parameters for Cr(VI) ions onto Dex-Fe_3O_4 nanocomposite at various concentrations of Cr(VI) ions and 30°C

Metal ion	Concentration (ppm)	Pseudo-first-order			Pseudo-second-order			Intraparticle		
		$q_{e,cal}$	k_1	R^2	$q_{e,cal}$	k_2	R^2	K_{int}	C	R^2
Cr(VI)	10 (q_{exp} = 9.88 mg g^{-1})	6.08	0.015	0.98	10.37	0.006	0.99	0.38	3.79	0.89
	50 (q_{exp} = 18.56 mg g^{-1})	8.39	0.016	0.98	19.12	0.006	0.99	0.54	10.03	0.87
	100 (q_{exp} = 31.77 mg g^{-1})	10.69	0.017	0.98	32.15	0.008	0.99	0.56	23.08	0.77

adsorbed at equilibrium (mg g^{-1}) and q_t is the amount of Cr(VI) at any time t (mg g^{-1}). The linear plot of pseudo-second-order model is given in Fig. 16 from which constant k_2 and q_e can be calculated.

The calculated data for both the models are listed in Table 2 from which it can be that the correlation factor obtained for pseudo-second-order model (0.99) is higher than the pseudo-first-order (0.98) which showed that the experimental data for adsorption of Cr(VI) onto Dex-Fe_3O_4 nanocomposite was best fitted with pseudo-second-order model than the pseudo-first-order and furthermore. Moreover, the calculated values of q_e using pseudo-second-order rate equation and the experimental values were close to each other for all the concentrations studied as compared to pseudo-first-order rate equation which showed a large deviation from the experimental values indicating that adsorption kinetics for the uptake of Cr(VI) by Dex-Fe_3O_4 nanocomposite is best described by pseudo-second-order rate equation.

Intraparticle diffusion model determines the rate-determining steps of the adsorption process and is best described by the intraparticle model given by Weber and Morris [35]:

$$q_t = k_{int} t^{0.5} + C \quad (9)$$

where the parameter q_t is the amount adsorbed at time t (mg g^{-1}), K_{int} is the intraparticle diffusion equation constant (mg g^{-1} $min^{-1/2}$) and t is the time. According to the Weber–Morris model, the plot of q_t against $t^{1/2}$ should give a straight line when diffusion plays a role in the sorption rate and should cross the origin if intraparticle diffusion is the rate-determining step. From the Fig. 17, it was observed that the plot of q_t vs. $t^{1/2}$ was not a straight line and did not pass through the origin, moreover, poor values of correlation coefficients were obtained for 10, 50, and 100 mg L^{-1}, respectively (Table 2). This showed that the intraparticle diffusion was not the rate-determining factor in the adsorption of Cr(VI) onto Dex-Fe_3O_4 nanocomposite.

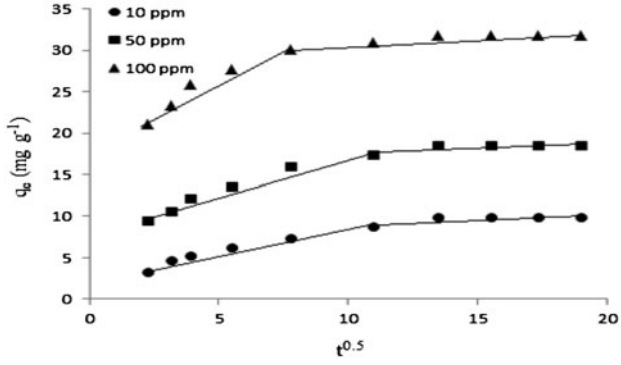

Fig. 17. Intraparticle diffusion model plot for removal of Cr(VI) onto Dex-Fe_3O_4 nanocomposite at various metal ion concentrations with 50-mg adsorbent dose and pH 2 at 30°C.

3.5. Adsorption thermodynamics

To observe the inherent energetic changes during the adsorption process, thermodynamic studies were carried out at 30, 40, and 50°C according to van't Hoff equation [36]:

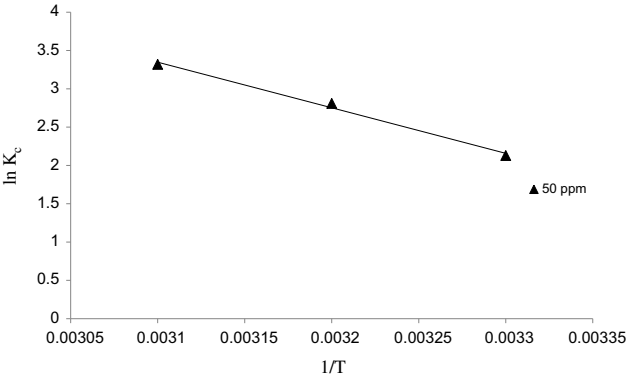

Fig. 18. Thermodynamic plot for Cr(VI) on Dex-Fe_3O_4 nanocomposite at 30, 40, and 50°C temperatures taking 50 mg of adsorbent dosage and 20 mL of 50 mg L^{-1} metal ion concentration at pH 2.

Table 3
Comparison of adsorption capacity of various adsorbents

Adsorbent	Adsorption capacity (mg g^{-1})	Refs.
SDS-activated charcoal	5.22	[37]
Sugarcane bagasse	13.72	[38]
Solvent-impregnated resin	28.2	[39]
Fe_3O_4/chitosan	39.61	[40]
Imidazole-silica	47.79	[41]
Alginate-montmorillonite/polyaniline	28.89	[42]
Dextrin/Fe_3O_4	71.43	This study

$$\ln K_c = -\frac{\Delta H^\circ}{R} + \frac{\Delta S^\circ}{RT} \quad (10)$$

The gas constant R is defined by 8.3145 J mol^{-1} K^{-1}; K_c (C_{ad}/C_e) is the distribution coefficient; and T is the temperature of the solution in Kelvin. ΔH° (kJ mol^{-1}) and ΔS° (JK^{-1} mol^{-1}) were calculated from the slope and intercept of a plot of ln K_c as a function of $1/T$, as shown in Fig. 18. The free energy change (ΔG°) can be determined from the following equation.

$$\Delta G^\circ = \Delta H^\circ - T\Delta S^\circ \quad (11)$$

It was observed that the positive value of ΔH° (49.47 kJ mol^{-1}) demonstrates the endothermic nature of adsorption of Cr(VI) onto Dex-Fe_3O_4 nanocomposite and the positive value of ΔS° (180.66 J K^{-1}) reveals the increased randomness at the solid/liquid interface during the sorption of Cr(VI) onto Dex-Fe_3O_4 nanocomposite which reflects the fact that chromium has a good affinity for Dex-Fe_3O_4. The values of ΔG° at 30, 40, and 50°C are −5.27, −7.07, and −8.88 suggesting that the adsorption process on Dex-Fe_3O_4 is spontaneous and the magnitude of the Gibbs free energy increased with increasing temperatures, indicating that better adsorption capacity of Dex-Fe_3O_4 for Cr(VI) can be obtained at higher temperatures.

3.6. Comparison of adsorption capacity

The comparison of adsorption capacities of various adsorbents has been presented in Table 3. It is evident from the table that present adsorbent exhibits the highest adsorption capacity of 71.43 mg g^{-1}.

4. Conclusions

Fe_3O_4 MNPs have been successfully incorporated in the polymer matrix which was further confirmed by FTIR, XRD, TGA, DTG, SEM, and TEM analysis. Dex-Fe_3O_4 nanocomposite has been found very effective and efficient for the removal of Cr(VI) from aqueous solution and the highest adsorption capacity of 17.8 mg g^{-1} was observed at pH 2. Adsorption of Cr (VI) onto Dex-Fe_3O_4 nanocomposite was spontaneous, endothermic and accompanied with an increase in entropy. The adsorption process followed the Langmuir adsorption model at different temperature ranges giving a maximum adsorption capacity of 51.43 at 30°C, 54.64 at 40°C and 71.43 at 50°C. The adsorption process was better described by the pseudo-second-order kinetic model than other kinetic models with high correlation coefficients over various concentration ranges of Cr(VI) ions (10, 50, and 100 mg L^{-1}). Therefore, it is concluded that Dex-Fe_3O_4 nanocomposite can be successfully utilized for the adsorption of Cr(VI) ions from aqueous solution.

Acknowledgement

The authors gratefully acknowledge the instrumentation laboratory, centre for excellence in nanomaterials Department of applied physics AMU, Sophisticated Analytical instrumentation facility (SAIF) Punjab University Chandigarh and highly thankful to UGC-MANF Delhi for providing financial assistance.

References

[1] H. Li, J. Li, Z. Chi, W. Ke, Kinetic and equilibrium studies of chromium(III) removal from aqueous solution by IRN-77 cation-exchange resin, Procedia Environ. Sci. 16 (2012) 646–655.
[2] S. Chen, Q. Yue, B. Gao, X. Xu, Equilibrium and kinetic adsorption study of the adsorptive removal of Cr(VI) using modified wheat residue, J. Colloid Interface Sci. 349 (2010) 256–264.
[3] M. Jain, V.K. Garg, K. Kadirvelu, Adsorption of hexavalent chromium from aqueous medium onto carbonaceous adsorbents prepared from waste biomass, J. Environ. Manage. 91 (2010) 949–957.

[4] S. Kocaoba, G. Akcin, Removal and recovery of chromium and chromium speciation with MINTEQA2, Talanta 57 (2002) 23–30.
[5] Y. Pang, G. Zeng, L. Tang, Y. Zhang, Y. Liu, X. Lei, Z. Li, J. Zhang, Z. Liu, Y. Xiong, Preparation and application of stability enhanced magnetic nanoparticles for rapid removal of Cr(VI), Chem. Eng. J. 175 (2011) 222–227.
[6] Z.A. AL-Othman, R. Ali, Mu. Naushad, Hexavalent chromium removal from aqueous medium by activated carbon prepared from peanut shell: Adsorption kinetics, equilibrium and thermodynamic studies. Chem. Eng. J. 184 (2012) 238–247.
[7] Z.A. AL-Othman, M. Naushad, R. Ali, Kinetic equilibrium isotherm and thermodynamic studies of Cr(VI) adsorption onto low-cost adsorbent developed from peanut shell activated with phosphoric acid. Environ. Sci. Pollut. Res. 20 (2013) 3351–3365.
[8] K. Shin, J. Hong, J. Jang, Heavy metal ion adsorption behavior in nitrogen-doped magnetic carbon nanoparticles: Isotherms and kinetic study, J. Hazard. Mater. 190 (2011) 36–44.
[9] M. Naushad, A. Mittal, M. Rathore, V. Gupta, Ion-exchange kinetic studies for Cd(II), Co(II), Cu(II) and Pb(II) metal ions over a composite cation exchanger, Desalin. Water Treat. 54(10) (2015) 2883–2890.
[10] H. Daraei, A. Mittal, M. Noorisepehr, J. Mittal, Separation of chromium from water samples using eggshell powder as a low-cost sorbent: Kinetic and thermodynamic studies, Desalin. Water Treat. 53(1) (2015) 214–220.
[11] M.A. Tofighy, T. Mohammadi, Adsorption of divalent heavy metal ions from water using carbon nanotube sheets, J. Hazard. Mater. 185 (2011) 140–147.
[12] V.K. Gupta, R. Jain, T.A. Saleh, A. Nayak, S. Malathi, S. Agarwal, Equilibrium and thermodynamic studies on the removal and recovery of safranine-T dye from industrial effluents, Sep. Sci. Technol. 46 (2011) 839–846.
[13] H. Daraei, A. Mittal, J. Mittal, H. Kamali, Optimization of Cr(VI) removal onto biosorbent eggshell membrane: Experimental and theoretical approaches, Desalin. Water Treat. 52(7–9) (2014) 1307–2315.
[14] G. Sharma, M. Naushad, D. Pathania, A. Mittal, G.E. El-desoky, Modification of *Hibiscus cannabinus* fiber by graft copolymerization: Application for dye removal, Desalin. Water Treat. 54 (2015) 3114–3121.
[15] Q. Liu, T. Zheng, P. Wang, J. Jiang, N. Li, Adsorption isotherm, kinetic and mechanism studies of some substituted phenols on activated carbon fibers, J. Chem. Eng. 157 (2009) 348–356.
[16] W. Gao, M. Majumder, L. Alemany, T.N. Narayanan, M.A. Ibarra, B.K. Pradhan, P.M. Ajayan, Engineered graphite oxide materials for application in water purification. ACS Appl. Mater. Interfaces 3 (2011) 1821–1826.
[17] H.Y. Zhu, R. Jiang, L. Xiao, G.M. Zeng, Preparation, characterization, adsorption kinetics and thermodynamics of novel magnetic chitosan enwrapping nanosized γ-Fe_2O_3 and multi-walled carbon nanotubes with enhanced adsorption properties for methyl orange, Bioresour. Technol. 101 (2010) 5063–5069.
[18] A. Józefczak, A. Skumiel, Ultrasonic investigation of magnetic nanoparticles suspension with PEG biocompatible coating, J. Magn. Magn. Mater. 323 (2011) 1509–1516.
[19] J. Mittal, A. Mittal, Hen feather a remarkable adsorbent for dye removal, in S.K. Sharma (Ed.), "Green Chemistry for Dyes Removal from Wastewater", Scrivener Publishing LLC, USA, California, (2015), pp. 409–857.
[20] G. Crini, Recent developments in polysaccharide-based materials used as adsorbents in wastewater treatment, Prog. Polym. Sci. 30 (2005) 38–70.
[21] K.S. Rajeev, S.C. Lalita, R. Ghanshyam, Verma, Graft copolymers of acrylonitrile onto dextrin for use in separation technologies, Int. J. Polym. Mater. Polym. Biomater. 59 (2010) 263–285.
[22] D.M. Silva, C. Nunes, I. Pereira, A.S. Moreira, M.R. Domingues, M.A. Coimbra, F.M. Gama, Structural analysis of dextrins and characterization of dextrin-based biomedical hydrogels, Carbohydr. Polym. 114 (2014) 458–466.
[23] D. Hritcu, D. Humelnicu, G. Dodi, M.I. Popa, Magnetic chitosan composite particles: Evaluation of thorium and uranyl ion adsorption from aqueous solutions, Carbohydr. Polym. 87 (2012) 1185–1191.
[24] Z.P. Yang, X.Y. Gong, C.J. Zhang, Recyclable Fe_3O_4/hydroxyapatite composite nanoparticles for photocatalytic applications, Chem. Eng. J. 165 (2010) 117–121.
[25] H.R.Wang, K.M.Chen, Preparation and surface active properties of biodegradable dextrin derivative surfactants, Colloids Surf., A: Physio. Eng. Aspects 281 (2006) 190–193.
[26] K. Ba, C. Blecker, S. Danthine, E. Tine, J. Destain, P. Thonart, Physicochemical characterization of dextrins prepared with amylases from sorghum malt, Starch/Stärke 65 (2013) 962–968.
[27] O. Ajouyed, C. Hurel, M. Ammari, L.B. Allal, N. Marmier, Sorption of Cr(VI) onto natural iron and aluminum (oxy)hydroxides: Effects of pH, ionic strength and initial concentration, J. Hazard. Mater. 174 (2010) 616–622.
[28] M. Monier, D.M. Ayad, A.A. Sarhan, Adsorption of Cu (II), Hg(II), and Ni(II) ions by modified natural wool chelating fibers, J. Hazar. Mater. 176 (2010) 348–355.
[29] A.G. Yavuz, E. Dincturk-Atalay, A. Uygun, F. Gode, E. Aslan, A comparison study of adsorption of Cr(VI) from aqueous solutions onto alkyl-substituted polyaniline/chitosan composites, Desalination 279 (2011) 325–331.
[30] L. Dagang, L. Zehui, L. Wei, Z. Zhengrong, X. Jianqiang, R. Jinjing, M. Zhongshi, Adsorption behaviour of heavy metal ions from aqueous solution by soy protein hollow microspheres, Ind. Eng. Chem. Res. 52 (2013) 11036–11044.
[31] I. Langmuir, The adsorption of gases on plane surfaces of glass, mica and platinum, J. Am. Chem. Soc. 40 (1918) 1361–1403.
[32] H.M.F. Freundlich, Over the adsorption in solution, Z. Phys. Chem. 57 (1906) 385–470.
[33] M.M. Dubinin, The potential theory of adsorption of gases and vapors for adsorbents with energetically nonuniform surfaces, Chem. Rev. 60 (1960) 235–241.
[34] R.N.Goyal, A.Kumar, A.Mittal, Oxidation chemistry of adenine and hydroxyadenines at pyrolytic graphite electrodes, J. Chem. Soc., Perkin Trans. 2 9 (1991) 1369–1375.

[35] W.J. Jr. Weber, J.C. Morris, Kinetics of adsorption on carbon from solution. J. Am. Soc. Civil Eng. 89 (1963) 31–59.
[36] B.H. Hameed, A.A. Ahmad, Batch adsorption of methylene blue from aqueous solution by garlic peel, an agricultural waste biomass, J. Hazard. Mater. 164 (2009) 870–875.
[37] U.E. Chaudhary, A.K. Wanjari, Sodium dodecyl sulfate impregnated granulated activated charcoal for the scavenging of Cr(VI) metal ions from aqueous solution, Int. J. Chem. Phys. Sci. 4 (2015) 261–266.
[38] Y. Zhu, H. Zhang, H. Zeng, M. Liang, R. Lu, Adsorption of chromium(VI) from aqueous solution by the iron(III)-impregnated sorbent prepared from sugarcane bagasse, J. Environ. Sci. Technol. 9 (2012) 463–472.
[39] N. Van Nguyen, J. Lee, J. Jeong, B.D. Pandey, Enhancing the adsorption of chromium(VI) from the acidic chloride media using solvent impregnated resin (SIR), Chem. Eng. J. 219 (2013) 174–182.
[40] M.R. Samarghandi, G. Asgari, A. Ahmadzadeh, A. Poormohammadi, M. Ahmadian, Fe_3O_4 magnetite nanoparticles synthesis and modified with chitosan biopolymers for removal of hexavalent chromium from aqueous solutions, J. Chem. Pharma. Res. 7 (2015) 933–941.
[41] Z. Wang, C. Ye, X. Wang, J. Li, Adsorption and desorption characteristics of imidazole-modified silica for chromium(VI), Appl. Surf. Sci. 287 (2013) 232–241.
[42] A. Olad, F. Farshi Azhar, A study on the adsorption of chromium (VI) from aqueous solutions on the alginate-montmorillonite/polyaniline nanocomposite, Desalin. Water Treat. 52 (2014) 2548–2559.